American Mineralogist, Volume 88, pages 293–300, 2003

Pressure-induced phase transition in malayaite, $CaSnOSiO_4$

STEPHANIE RATH,[1,*] MARTIN KUNZ,[2] AND RONALD MILETICH[3]

[1]Labor für Kristallographie, ETH Zürich, Sonneggstrasse 5, CH-8092 Zürich, Switzerland
[2]Museum of Natural History, Augustinergasse 2, CH-4001 Basel, and Department of Earth Sciences, University of Basel, Bernoullistrasse 30, CH-4056 Basel, Switzerland
[3]Mineralogisches Institut, Universität Heidelberg, Im Neuenheimer Feld 236,D-69120 Heidelberg, Germany

ABSTRACT

A single crystal high-pressure diffraction study in a diamond-anvil cell shows that monoclinic malayaite ($CaSnOSiO_4$) transforms into a triclinic high-pressure polymorph at $P_c = 4.95(1)$ GPa. No discontinuity was observed for the individual crystallographic axes or the volume compressibility. Instead, the $A2/a - A\bar{1}$ phase transition reveals itself by significant deviations of the α and γ angles from 90°. The bulk elastic properties of the triclinic phase cannot be distinguished from those of the monoclinic structure within experimental uncertainty ($A2/a$: $V_0 = 389.68(3)$ Å^3, $K_0 = 121(1)$ GPa, and $K' = 4.2(5)$; $A\bar{1}$: $V_0 = 390.3(1)$ Å^3, $K_0 = 118.3(7)$ GPa, $K' = 4$). Fitting the compressibility to all data gives values of $V_0 = 389.64(3)$ Å^3, $K_0 = 121.6(7)$ GPa and $K' = 4.6(2)$. Structure refinements at four different pressures reveal the structural details of the monoclinic $A2/a$ and triclinic $A\bar{1}$ phases. Below the transition temperature the SiO_4 polyhedra show some non-rigid distortion, whereas the SnO_6 polyhedra remain almost unchanged. At the phase transition, the SiO_4 tetrahedra show further angular twisting while the SnO_6 chains shift parallel to $[\bar{1}01]$, inducing a reduction in symmetry. Furthermore, at pressures above 5 GPa the Ca atoms are displaced almost parallel to [100], causing a change in coordination from CaO_7 polyhedra to sheets of CaO_8 parallel to $(\bar{1}11)$.

At 7.394(4) GPa the cell parameters of the triclinic structure are $a = 6.9958(4)$ Å, $b = 8.8080(9)$ Å, $c = 6.4968(4)$ Å, $\alpha = 89.078(7)°$, $\beta = 112.745(5)°$, $\gamma = 91.230(7)°$, $V = 369.10(5)$ Å^3; space-group $A\bar{1}$.

INTRODUCTION

The mineral malayaite, $CaSnOSiO_4$, was first described from an occurrence in Perak, Malay Peninsula (Ingham and Bradford 1961). The structure of the colorless to yellowish mineral was solved by Higgins and Ribbe (1976) in space group $A2/a$. They showed that the structure of malayaite is characterized by SnO_6-octahedra forming chains parallel to [100] through shared *trans* corners. These chains are mutually connected via SiO_4 tetrahedra. CaO_7 polyhedra form chains parallel to [101] within the SnO_6-SiO_4 framework (Fig. 1). This structure is equivalent to the aristotype of titanite $CaTiOSiO_4$. Takenouchi (1971) showed that malayaite and titanite have a complete solid solution above 888 ± 15K. Kunz et al. (1997) investigated the $CaSnOSiO_4$–$CaTiOSiO_4$ join in more detail using quenched samples and found that a small substitution (10 mol%) of Sn changes the titanite symmetry from $P2_1/a$ to $A2/a$. Investigations of malayaite at high temperature using synchrotron radiation, high-resolution transmission electronic microscopy, X-ray powder diffraction, and Raman spectroscopy by Groat et al. (1996) revealed a structural anomaly around 500 K. The authors correlated this anomaly with the thermal parameter of the Ca position indicating a maximum elongation along the **a** axis. Nevertheless, they did not find any deviations from $A2/a$ symmetry, nor any structural domains or antiphase boundaries with a reduced symmetry. Meyer et al. (1998) reinvestigated the 500 K anomaly using single crystal X-ray diffraction and powder IR spectroscopy at different temperatures. They confirmed the strong increase of the anisotropic thermal parameter U_{11} for Ca as a function of temperature and concluded a partial collapse of the CaO_7 polyhedra around 500 K. Both Bismayer et al. (1999) and Zhang et al. (1999) described another important behavior with respect to the 500 K anomaly: single crystal X-ray diffraction and powder hard-mode IR studies showed a weak tilting of the SnO_6 octahedra. These displacements changed the environment around the Ca atoms in that one O atom moved closer to the calcium atom. Zhang et al. (1999) also reported a change in the coordination of the Ca atom and described the structural anomaly at 500 K as an isosymmetric second-order phase transition.

As mentioned above, titanite $CaTiOSiO_4$ is isostructural to malayaite and has been an object of several investigations. At ambient conditions the Ti atoms exhibit out-of-center distortions with parallel displacement vectors within a single TiO_6 chain and antiparallel orientation between neighboring chains. High-temperature studies of titanite showed a phase transition from $P2_1/a$ to $A2/a$ symmetry (α-β transition) at 496 K (Taylor and Brown 1976; Kek et al. 1997; Salje et al. 1993). The transition at 496 K is driven by the loss of long-range coherence between the out-of-center dipoles due to a dynamic disorder with increasing temperatures. Therefore the structure shows on average $A2/a$ symmetry. A second, isosymmetric phase transition has been observed at 825 K and ambient pressure (β-γ

* Current adress: Christian-Albrechts-Universität zu Kiel, Institut für Geowissenschaften, Mineralogie, Ludewig-Meyn-Strasse 10, D-24118 Kiel. E-mail: srath@min.uni-kiel.de

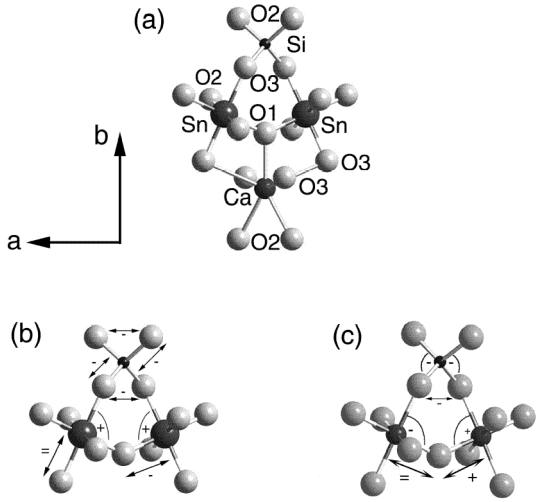

FIGURE 1. (**a**) Ball and stick model of a fragment of the malayaite structure. (**b**) Same fragment in the monoclinic phase at 4.505 GPa and (**c**) in the triclinic phase at 7.33 GPa.

transition) (Kek et al. 1997; Zhang et al. 1997; Chrosch et al. 1997). Malcherek (2001) used spontaneous strains calculated from high-temperature powder data to show that the intermediate phase between 496 and 825 K is characterized by shearing. High-pressure powder experiments (Angel et al. 1999; Kunz et al. 1996) also revealed a phase transition at 3.5 GPa corresponding to a symmetry change from $P2_1/a$ to $A2/a$. Kunz et al. (2000) related the 825 K phase transition to the 3.5 GPa phase transition based on their in situ powder diffraction study under simultaneous high pressure and high temperature. The high-pressure phase as well as the high temperature γ-phase are assumed to be induced by local symmetrization of the Ti octahedra, i.e., a disappearance of its out-of-center distortion.

The close structural relationship between malayaite and titanite invites an investigation into the influence of electronic effects on structural phase transitions. While the known phase transitions in titanite are apparently dominated by the interaction of the 2nd order Jahn-Teller distorted, octahedrally coordinated d^0 transition metal Ti^{4+}(Munowitz et al. 1993), is replaced by Sn^{4+}. A study of the *P-T* behavior of malayaite may therefore provide insight into the relative importance of electronic vs. topological effects on structural stability. In this study we focus on the compressional behavior of malayaite and its pressure-induced phase transformation.

EXPERIMENTAL METHODS

The malayaite samples for this experiment were taken from the same sample used by Groat et al. (1996), Meyer et al. (1998), and Bismayer et al. (1999). Its origin is a skarn north of Ash Mountain in British Columbia (Canada). The sample has the following chemical composition based on five O atoms according to Bismayer et al. (1999): $Ca_{1.01}Sn_{1.01}Fe_{0.01}Si_{0.98}O_5$.

Two different single crystals of malayaite were used for the high-pressure experiments. The first crystal was pressurized from ambient conditions up to 7.394(4) GPa. At ~7.6 GPa the crystal bridged the diamond anvils and broke apart. Another crystal was loaded for both intensity measurements and additional compressibility data points in the range of interest. Both single crystals of malayaite, with dimensions $100 \times 80 \times 80$ μm^3 and $130 \times 50 \times 40$ μm^3, respectively, were mounted into a ETH diamond-anvil cell (Miletich et al. 2000) using a 4:1 methanol-ethanol mixture as hydrostatic pressure medium. Stainless steel gaskets were preindented to 80–100 μm and a hole 250 μm in diameter served as the pressure chamber. A small ruby and a quartz crystal were loaded into the cell as pressure calibrants. Accurate pressures were determined from the unit-cell volumes of the quartz crystal using the equation of state reported by Angel et al. (1997) yielding errors ranging from 0.003 to 0.02 GPa. The ruby crystal was used for in-situ pressure determination during the pressure setting (Mao et al. 1986). A total of 34 pressure points were collected on a Huber four-circle diffractometer (unfiltered Mo radiation, 45kV, 35mA) with a point detector in a pressure range from room pressure to ~7.4 GPa using the 8-position-centering technique (King and Finger 1979). Intensity data were collected with an Enraf Nonius CAD4 diffractometer (graphite-monochromatized Mo$K\alpha$ radiation, 50 kV, 30 mA) at 4.238(4), 4.505(7), 5.769(5), and 7.33(2) GPa. The measured reflections were filtered through the program Integrate (R. Angel, personal communication), where each single reflection was surveyed in order to reject aberrant reflections, which were contaminated by signals from the cell components. Peak fits were performed using the Lehmann-Larsen algorithm (Grant and Gabe 1978). An analytical absorption correction for both sample and beam path through the cell was performed using the program Absorb modified after Burnham (1966). Using the remaining reflections with $I > 4\sigma$, the structures were refined with Shelx-97 (Sheldrick 1997) yielding *R* factors between 5.69% (ambient conditions) and 7.27% (4.238 GPa). The refinement in the triclinic phase with $P_c > 5$ GPa was done in space group $A\bar{1}$. We chose $A\bar{1}$ instead of the standard $P\bar{1}$ in order to more easily compare the triclinic structure with the monoclinic $A2/a$ structure. In order to transform coordinates from the $A\bar{1}$ setting into $P\bar{1}$, the following matrix was applied: $\begin{pmatrix} 1 & 0 & 0 \\ 0 & 1 & 1 \\ 0 & \bar{1} & 1 \end{pmatrix}$. During refinement, the displacement parameters for the O atoms were constrained to be equal. The Si–O bond lengths were soft-constrained to a target value of 1.64 Å (weighting factor 0.006). The angles were allowed to refine. The isotropic displacement parameters U_{iso} for the O atoms were fixed at 0.010 $Å^2$. For more details see Table 1.

RESULTS AND DISCUSSION

Refined unit-cell parameters for 35 different pressures including a data point from a crystal in air are given in Table 2. Fractional coordinates of atoms for five different pressure points are shown in Table 3. Selected bond lengths and interatomic distances are reported in Table 4. The compressibility results are summarized in Table 5.

TABLE 1. Structure refinement detail

P(GPa)	0.000(6)	4.238(7)	4.505(4)	5.769(5)	7.33(2)
Space Group	$A2/a$	$A2/a$	$A2/a$	$A\bar{1}$	$A\bar{1}$
a (Å)	7.1523(4)	7.0560(3)	7.0498(4)	7.0252(2)	6.9948(4)
b (Å)	8.8902(5)	8.8436(7)	8.8402(8)	8.8281(4)	8.8103(9)
c (Å)	6.6677(9)	6.5629(3)	6.5573(4)	6.5318(2)	6.4976(3)
α (°)	90	90	90	89.861(4)	89.175(6)
β (°)	113.362(7)	112.948(3)	112.925(4)	112.840(2)	112.738(4)
γ (°)	90	90	90	90.171(4)	91.104(6)
Total $\lvert F_{obs}\rvert$	2516	2491	1344	2482	2386
Averaged $\lvert F_{obs}\rvert$	981	903	1002	1191	1178
$\lvert F_{obs}\rvert$ $(F > 4\sigma_F)$	542	629	667	803	777
R_{int} (%)	2.57	1.91	1.92	2.43	1.55
t_{min} (%)	29.4	23.2	22.7	24.3	24.6
t_{max} (%)	38.9	31.6	33.3	33.3	33.4
N_{var}	14	14	14	27	27
R_1 (%)	5.68	7.27	5.93	7.01	6.59
GooF	1.25	1.05	0.92	1.16	1.77

Notes: t_{min} and t_{max} give the X-ray transmission percentage after its path through the cell and the sample. $R_{int} = \Sigma \lvert F_o^2 - F_{cmean}^2 \rvert / \Sigma [F_o^2]$; $R_1 = \Sigma \lvert F_o - F_c \rvert / \Sigma F_o$; GooF = $S = \{ \Sigma [w(F_o^2 - F_c^2]^2 / n - p\}$ with w = weights, n = numbers of reflections, and p = total number of parameters refined.

TABLE 2. Unit-cell parameters of malayaite at various pressures

P(GPa)	a (Å)	b (Å)	c (Å)	V (Å^3)	α	β	γ	$N_{Reflections}$
0.0001*	7.1529(5)	8.8901(5)	6.6667(5)	389.19(4)	90	113.359(4)	90	21
0.0001†‡	7.1556(7)	8.897(1)	6.6697(8)	389.23(5)	90	113.352(8)	90	11
0.09(1)	7.1532(4)	8.8964(6)	6.666(3)	389.51(4)	90	113.348(4)	90	27
0.52(1)	7.1406(3)	8.8899(7)	6.6541(3)	387.96(4)	90	113.297(3)	90	30
0.645(6)	7.1400(4)	8.8907(6)	6.6517(3)	387.86(4)	90	113.287(4)	90	26
1.074(7)	7.1297(4)	8.8851(6)	6.6403(3)	386.51(4)	90	113.246(4)	90	27
2.115(9)	7.1051(4)	8.8722(6)	6.6138(3)	383.37(4)	90	113.145(4)	90	26
3.001(5)	7.0837(2)	8.8575(4)	6.5916(2)	380.53(3)	90	113.064(3)	90	23
3.059(4)	7.0818(2)	8.8571(4)	6.5898(2)	380.34(3)	90	113.058(3)	90	26
3.987(5)	7.0619(2)	8.8475(6)	6.5690(3)	377.88(3)	90	112.973(3)	90	21
4.077(3)	7.0587(3)	8.8443(7)	6.5650(3)	377.38(4)	90	112.962(3)	90	20
4.165(4)	7.0580(4)	8.8446(8)	6.5650(4)	377.38(5)	90	112.954(4)	90	26
4.238(7)‡	7.0560(3)	8.8436(7)	6.5629(3)	377.12(4)	90	112.948(3)	90	21
4.254(5)	7.0559(2)	8.8437(3)	6.5634(2)	377.14(2)	90	112.953(2)	90	27
4.407(5)	7.0526(2)	8.8436(3)	6.5605(2)	376.83(2)	90	112.938(2)	90	26
4.505(4)‡	7.0498(4)	8.8402(8)	6.5573(4)	376.38(4)	90	112.925(4)	90	26
4.572(4)	7.0486(4)	8.8401(8)	6.5559(4)	376.27(5)	90	112.916(4)	90	27
4.955(5)	7.0417(2)	8.8374(4)	6.5488(2)	375.44(3)	90	112.895(3)	90	27
5.257(7)	7.0355(2)	8.8338(3)	6.5430(3)	374.68(3)	89.929(4)	112.873(3)	90.079(4)	27
5.351(9)	7.031(8)	8.829(1)	6.5413(6)	374.09(8)	89.902(5)	112.900(7)	90.137(5)	18
5.56(1)	7.0293(3)	8.8309(5)	6.5357(3)	373.88(4)	89.892(3)	112.846(4)	90.133(3)	31
5.611(5)	7.0285(2)	8.8296(3)	6.5350(1)	373.75(2)	89.877(5)	112.847(3)	90.148(5)	30
5.68(1)	7.0270(4)	8.8297(4)	6.5345(4)	373.67(3)	89.897(7)	112.835(4)	90.165(7)	26
5.694(5)	7.0266(2)	8.8282(6)	6.5330(3)	373.49(4)	89.866(5)	112.838(3)	90.157(5)	27
5.769(5)‡	7.0252(2)	8.8281(4)	6.5318(2)	373.34(2)	89.861(4)	112.840(2)	90.171(4)	26
5.842(7)	7.0245(6)	8.8251(7)	6.5314(5)	373.18(5)	89.737(7)	112.824(6)	90.389(7)	26
5.991(7)	7.0203(3)	8.8260(6)	6.5269(3)	372.76(4)	89.734(7)	112.819(4)	90.346(8)	28
6.106(6)	7.0185(4)	8.8257(7)	6.5246(4)	372.54(5)	89.660(8)	112.813(5)	90.449(7)	23
6.292(5)	7.0161(7)	8.8191(7)	6.5203(6)	371.88(5)	89.490(7)	112.804(6)	90.686(8)	24
6.435(5)	7.0132(6)	8.8171(6)	6.5166(6)	371.45(5)	89.420(7)	112.793(6)	90.779(7)	24
6.600(6)	7.0085(3)	8.8194(6)	6.5141(3)	371.21(4)	89.452(6)	112.781(4)	90.732(6)	23
6.97(1)	7.0026(4)	8.8157(11)	6.5073(4)	370.38(6)	89.321(7)	112.761(4)	90.906(7)	27
7.104(5)	7.0008(3)	8.8100(3)	6.5032(3)	369.80(2)	89.159(3)	112.755(3)	91.123(3)	27
7.33(2)‡	6.9948(3)	8.8102(9)	6.4976(3)	369.23(5)	89.175(6)	112.738(4)	91.104(6)	27
7.394(4)	6.9958(4)	8.8080(9)	6.4968(4)	369.10(5)	89.078(7)	112.745(5)	91.230(7)	26

* Crystal in air.
† Crystal in DAC.
‡ Structural data collected at this pressure.

Structural phase transition

A structural phase transition accompanied by a symmetry reduction from monoclinic to triclinic revealed itself at P_c = 4.95(1) GPa. At this pressure the α and γ angles begin to deviate from 90°, and reached maximum values of 91.230(7)° and 89.078(7)°, respectively, at 7.33(2) GPa (Fig. 2). No discontinuity was observed in the pressure dependence of axes and volume. The phase transition is fully reversible. However, we observe a reproducible, conspicuous change in slope in the evolution of the α and γ angle with pressure within the triclinic phase around ~5.7 GPa.

Compressibility

The bulk modulus of malayaite was determined by fitting a Birch-Murnaghan equation of state (Eq. 1) to the P-V data of the monoclinic phase:

$$P = \frac{3}{2} * K_0 \left[\left(\frac{V_0}{V} \right)^{\frac{7}{3}} - \left(\frac{V_0}{V} \right)^{\frac{5}{3}} \right] * \left\{ 1 - \frac{3}{4} * \left(4 - K' \right) * \left[\left(\frac{V_0}{V} \right)^{\frac{2}{3}} - 1 \right] \right\} \quad (1)$$

Least squares fits yield V_0 = 389.68(3)Å^3, K_0 = 121(1) GPa and K' = 4.2(5) for data with $P < P_c$. For data with $P > P_c$ K' has been fixed to 4 as this value is generally accepted for silicates.

TABLE 3. Fractional atomic coordinates of malayaite at various pressures

P (GPa)	atom	*x*	*y*	*z*	U_{iso} (Å^2)
1 bar	Ca	0.25	0.6628(5)	0.5	0.025(1)
	Sn	0.5	0.5	0.0	0.009(3)
A2/a	Si	0.75	0.6815(5)	0.5	0.0107(9)
	O1	0.75	0.587(1)	0.0	0.010
	O2	0.9147(9)	0.5679(8)	0.676(1)	0.010
	O3	0.370(2)	0.7116(9)	0.888(4)	0.010
4.238(7)	Ca	0.25	0.6607(8)	0.5	0.0260(8)
	Sn	0.5	0.5	0.0	0.0097(3)
A2/a	Si	0.75	0.6834(8)	0.5	0.0105(7)
	O1	0.75	0.591(2)	0.0	0.010
	O2	0.9177(9)	0.568(1)	0.672(1)	0.010
	O3	0.370(1)	0.711(1)	0.887(1)	0.010
4.505(4)	Ca	0.25	0.6608(7)	0.5	0.0276(7)
	Sn	0.5	0.5	0.0	0.0101(3)
A2/a	Si	0.75	0.6823(6)	0.5	0.0101(6)
	O1	0.75	0.588(2)	0.0	0.010
	O2	0.9179(7)	0.569(1)	0.6722(9)	0.010
	O3	0.3700(8)	0.712(1)	0.8864(9)	0.010
5.769(5)	Ca	0.2462(6)	0.662(1)	0.502(1)	0.0283(7)
$A\bar{1}$	Sn	0.5	0.5	0.0	0.0114(3)
	Sn2	0.0	0.5	0.0	0.0116(3)
	Si	0.7494(6)	0.682(1)	0.499(1)	0.0121(6)
	O1	0.753(1)	0.589(3)	0.002(2)	0.010
	O2	0.919(1)	0.568(2)	0.671(2)	0.010
	O2.2	–0.419(1)	0.567(2)	–0.673(2)	0.010
	O3	0.370(1)	0.712(3)	0.886(2)	0.010
7.33(2)	Ca	0.2311(5)	0.659 (1)	0.5047(8)	0.0287(7)
$A\bar{1}$	Sn	0.5	0.5	0.0	0.0136(3)
	Sn2	0.0	0.5	0.0	0.0135(3)
	Si	0.7440(5)	0.683(1)	0.4972(9)	0.0149(7)
	O1	0.7561(9)	0.587(2)	0.004(1)	0.010
	O2	0.9229(8)	0.575(1)	0.670(1)	0.010
	O2.2	–0.4173(9)	0.565(2)	–0.670(1)	0.010
	O3	0.3730(9)	0.714(2)	0.886(1)	0.010
	O3.2	0.1341(9)	0.710(2)	–0.879(1)	0.010

Furthermore, it is close to the fitted K' of the low-pressure phase. Least square fits yield values of $V_0 = 390.3(1)$ Å^3, $K_0 = 118.3(7)$ GPa, $K' = 4$ (fixed) for data with $P > P_c$. This implies a softening of the structure under high pressure, which is impossible from a thermodynamic point of view. As the difference of the fitted compressibility values is less than two standard deviations we conclude that the resolution of our data does not allow us to detect any difference in elastic properties between the monoclinic and triclinic phase. We therefore applied a single EoS to the full pressure range from room pressure to 7.3 GPa. Fitting a third order Birch-Murnaghan equation of state to these data yields the following values: V_0 = 389.64(3) Å^3, K_0 = 121.6(7) GPa, and K' = 4.6(2). The K_0 of *A*2/*a* malayaite is smaller than that of titanite [120(1) GPa vs. 131.4(7) GPa], which means that malayaite is easier to compress than titanite (Table 5).

Due to the above-mentioned kink in the α and γ angles at 5.7 GPa, an attempt was made to fit bulk and axial compressibilities as well as angle-polynomials separately to data above and below 5.7 GPa. No significant difference was obtained for axial values, whereas the observed angular kink is clearly reflected in the fitted polynomial. The axial compressibilities were calculated by Equation 2, where *K*' has been fixed at 4:

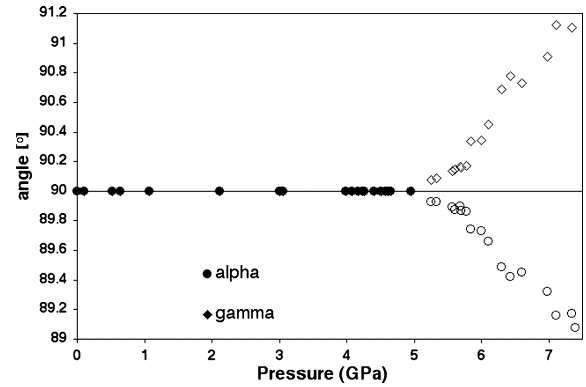

FIGURE 2. Evolution of the α (circles) and γ angle (diamonds) as a function of pressure. The experimental uncertainties are smaller than the symbols. Full symbols mark the angle before the phase transition, open symbols denote the angle after the phase transition. Note the change of the slope at ~5.8 GPa.

$$a = a_0 * \left(1 + \frac{4P}{K_0}\right)^{-1/12} \qquad (2)$$

In the *A*2/*a* phase, the **b** axis is the least compressible (Fig. 3), similar to titanite. More details of the respective axial compressibilities and bulk moduli are given in Table 5.

Structural evolution

In order to correlate the monoclinic to triclinic phase transition with structural changes we measured diffracted intensities on either side of the phase transition, namely at 4.238(4), 4.505(7), 5.769(5), and 7.33(2) GPa, respectively. The structure refinements reveal the following patterns:

Monoclinic. Between room pressure and 4.5 GPa the Sn-O1-Sn angle shows no significant change. At the same time a very small internal distortion of the SnO_6 octahedron (Table 4) is observed. The Sn-O bond distances remain almost constant (Table 4). This stiffness shows that the SnO_6 polyhedra act as rigid units inside the structure. Within the polyhedra only the expected shortening of the bond lengths can be seen. The greatest change in the monoclinic structure is in the SiO_4 tetrahedral edges (O3-O3 and O2-O2), which decrease by 0.02 and 0.036 Å, respectively (Table 4). At the same time, the Si-O bond distances decrease (Table 4). The tetrahedral angles remain nearly constant suggesting an isotropic compression of the SiO_4 tetrahedra. The large volume reduction of the CaO_7 polyhedra in the monoclinic phase (3.4%) makes it the softest structural unit. But, remarkably, the SiO_4 tetrahedron is forced to reduce its volume by about 3%, which is mainly achieved by a decrease in bond lengths. This soft behavior of the $[SiO_4]^{4-}$ complex anion relative to the other structural units is unusual and surprising.

Triclinic. The structural differences between the triclinic and monoclinic phase are most clearly recognized when looking at cation-cation distances. As mentioned above, in the monoclinic structure the SnO_6 octahedra form linear chains parallel to [100]. When projected parallel to [100] these chains are arranged on the corners of an even-sided rhombus with four equivalent Sn-Sn distances parallel to <011>. Above the phase transition, the distance between adjacent SnO_6 chains is com-

TABLE 4. Selected interatomic distances (Å) and angles (°) for $CaSnOSiO_4$ at different pressures

Pressure (GPa)	0.000(6)	4.238(7)	4.505(4)	5.769(5)	7.33 (2)
Space group	*A*2/*a*	*A*2/*a*	*A*2/*a*	$A\bar{1}$	$A\bar{1}$
Ca-O1	2.22(1)	2.20(2)	2.22(1)	2.20(2)	2.24(2)
Ca-O2	2.42(1)	2.40(1)	2.40(1)	2.40(2)	2.40(2)
Ca-O22				2.40(2)	2.39(1)
Ca-O3	2.42(2)	2.3856)	2.381(6)	2.36(2)	2.34(1)
Ca-O32				2.37(1)	2.356(7)
Ca-O3	2.755(9)	2.735(8)	2.728(6)	2.743(1)	2.794(9)
Ca-O32				2.69(1)	2.65(1)
Ca-O2	3.174(7)	3.084(7)	3.078(6)	3.024(8)	2.838(7)
<Ca-O>(Ca[7])	2.49(20)	2.46(20)	2.46(19)	2.45(19)	2.49(20) *
polyhedral	20.750	19.982	20.036	19.705	19.581
volume				26.082*	25.749*
Sn-O1 (2×)	1.949(4)	1.939(7)	1.927(5)	1.94(1)	1.926(7)
Sn-O2.2 (2×)	2.09(1)	2.088(6)	2.088(5)	2.07(2)	2.08(1)
Sn-O3 (2×)	2.10(1)	2.08(1)	2.092(9)	2.09(2)	2.10(1)
<Sn-O>	2.065(75)	2.035(75)	2.035(84)	2.033(72)	2.035(85)
O3-Sn-O1	94.4(5)	95.6(5)	95.0(4)	94.9(6)	94.2(5)
O3-Sn-O2	90.7(7)	90.9(4)	90.7(3)	91.0(6)	91.1(5)
Sn2-O2(2×)				2.085(8)	2.099(6)
Sn2-O1 (2×)				1.91(1)	1.90(1)
Sn2-O32 (2×)				2.10(2)	2.08(2)
<Sn2-O>				2.013(85)	2.000(82)
O32-Sn2-O1				95.9(8)	95.9(5)
O32-Sn2-O2				91.4(6)	90.9(4)
Sn-O1-Sn 2	133.2(6)	131.0(9)	132.4(7)	132(1)	132.6(9)
Polyhedral	11.350	11.191	11.172	11.140	11.178
volume				11.110	10.958
Si-O2	1.639(8)	1.635(7)	1.624(6)	1.630(7)	1.631(7)
Si-O22				1.63(2)	1.60(2)
Si-O3	1.64(1)	1.621(9)	1.623(8)	1.63(2)	1.61(2)
Si-O3.2				1.63(1)	1.631(9)
<Si-O>	1.6395(6)	1.6280(81)	1.6235(6)	1.630	1.618(15)
O2-Si-O22	104.0(8)	102.8 (7)	103.9(6)	103.4(9)	103.8(8)
O3-Si-O3	109.2(8)	109.7(8)	109.7(7)	110(1)	110.4(9)
O32-Si-O2	108.9(6)	108.0(4)	107.8(4)	107.5(5)	104.6(4)
O3-O3	2.68(1)	2.651(7)	2.654(6)	2.66(1)	2.663(7)
O2-O2	2.583(8)	2.556(8)	2.557(6)	2.56(1)	2.547(7)
Polyhedral	2.254	2.200	2.184	2.194	2.164
volume					

* These values are calculated for CaO_8 polyhedra in triclinic structures.

TABLE 5. Comparison of equations of state between malayaite ($CaSnOSiO_4$) and titanite ($CaTiOSiO_4$)

Malayaite			
*A*2/*a*		K_0 (GPa)	K'
Bulk compressibility	V_0 = 389.68(3) Å^3	121(1)	4.2(5)
Axial compressibilities	a_0 = 7.156(2) Å	93.0(5)	4 (fixed)
	b_0 = 8.8985(3) Å	226(3)	
	c_0 = 6.6695(3) Å	79.3(4)	
	$\beta_0 = 113.361(2) - 0.122(3)P + 0.0037(1)P^2$		
$A\bar{1}$			
Bulk compressibility	V_0 = 390.3(1) Å^3	118.3(7)	4
Axial compressibilities	a_0 = 7.154(1) Å	94.92(7)	
	b_0 = 8.8985(1) Å	229.2(4)	
	c_0 = 6.6697(1) Å	80.47(8)	
5.2 – 5.76 GPa	$\alpha_0 = 90.001(5) + 0.23(6)\Delta P + 0.09(7)\Delta P^2$		
	$\beta_0 = 112.896(4) - 0.08(1)\Delta P + 0.08(2)\Delta P^2$		
	$\gamma_0 = 90.001(5) - 0.026(2)\Delta P + 0.06(2)\Delta P^2$		
5.84 – 7.39 GPa	$\alpha_0 = 90.3(2) - 0.64(4)\Delta P + 0.070(2)\Delta P^2$		
	$\beta_0 = 112.88(1) - 0.062(3)\Delta P + 0.002(1)\Delta P^2$		
	$\gamma_0 = 89.6(3) + 0.89(6)\Delta P - 0.10(3)\Delta P^2$		
Titanite (Angel et al. 1999)		K_0 (GPa)	K'
Bulk compressibility	V_0 = 367.7(1)	131.4(7)	4 (fixed)
Axial compressibilities	a_0 = 7.046(1)	89.9(9)	
	b_0 = 8.707(5)	229(1)	
	c_0 = 6.5543(1)	90.65(8)	
	$\beta_0 = 113.84(1) - 0.141(4)P + 0.0041(3)P^2$		

Note: The axial compressibilities were fitted to the equation $x = x_0 * (1 + 4P/K_0)^{-1/12}$, where x and x_0 denote the unit-cell axes *a, b* and *c* at the measured and zero pressure, respectively. The monoclinic angle β was fitted to a second-degree polynomial. For the triclinic phase, only the α and γ angles were fitted separately above and below 5.7 GPa.

pressed more strongly parallel to [011] than parallel to [01$\bar{1}$], violating both the twofold screw axis and the glide plane (Table 6, Fig. 4). As a consequence, the Sn site splits into two symmetrically distinct sites occupying alternate positions along the octahedral chains. The asymmetric relative shift of the SnO_6 chains is also reflected in a twisting of the chain-linking SiO_4 tetrahedra. Their O2-O2 vector rotates relative to the O3-O3 edge to make a more parallel arrangement of these normally perpendicular tetrahedral edges.

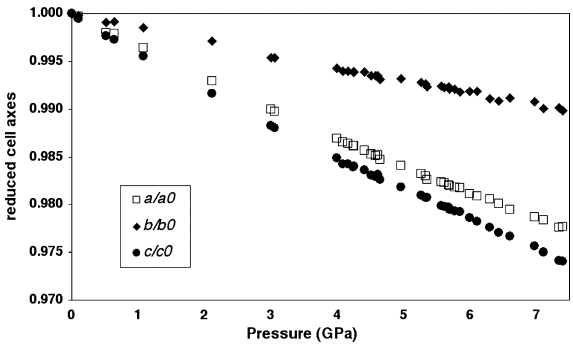

FIGURE 3. Reduced cell axes of malayaite as a function of pressure.

TABLE 6. Distances between Sn atoms parallel to <011>

Pressure (GPa)	0.000(6)	4.238(7)	4.505(4)	5.769(5)	7.33(2)
1	5.556 Å	5.506 Å	5.503 Å	5.485 Å	5.436 Å
2	5.556 Å	5.506 Å	5.503 Å	5.497 Å	5.511 Å
3	5.556 Å	5.506 Å	5.503 Å	5.485 Å	5.436 Å
4	5.556 Å	5.506 Å	5.503 Å	5.497 Å	5.511 Å
Sn – Sn	3.576 Å	3.528 Å	3.525 Å	3.513 Å	3.497 Å

Note: The numbers 1–4 refer to the labeling in Figure 4. Sn – Sn lists the distances within an octahedral chain. Note the stronger decrease parallel [011] (1 and 3) if compared to [011] (2 and 4).

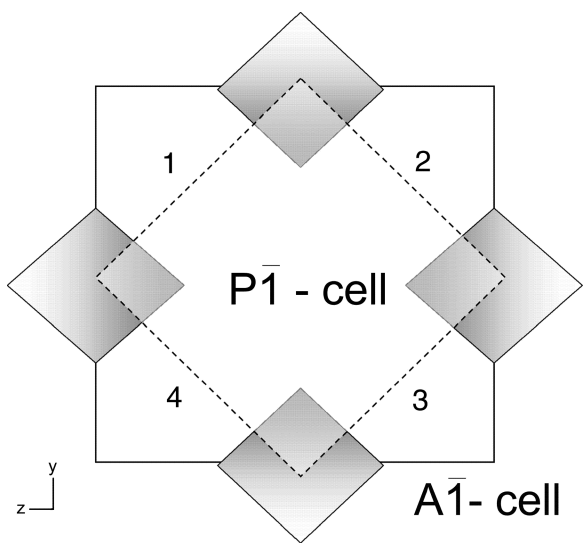

FIGURE 4. Schematic sketch of the $A\bar{1}$ (solid line) and $P\bar{1}$ (dashed line) setting for malayaite viewed along *a*. The diamonds represent the octahedral chains projected parallel to the *a* axis. The even-sided rhombohedral shape outlined by 4 neighboring chains becomes an uneven rhombus in the triclinic phase. The numbers denote the distances listed in Table 6.

The distortion of the SnO_6-SiO_4 framework also affects the coordination of the Ca atom. As a response to the imposed constraint due to high pressure, the CaO_7 polyhedra move closer together. This brings an eighth O atom (part of the neighboring CaO_7 polyhedra) into the coordination sphere of the Ca atom (Fig. 5a). The bond valence of this new Ca-O2 bond increases from 0.038 v.u. at 1 bar to 0.057 v.u. at 5.7 GPa to 0.095 v.u. at 7.3 GPa (Fig 5b). Hence the originally linear CaO_7 chains change into CaO_8 sheets parallel to ($\bar{1}$11) in the triclinic phase at 7.338 GPa (Fig. 6). It is remarkable that this polymerization does not coincide with the phase transition at 4.95(1) GPa but occurs somewhere within the triclinic phase. Comparing the evolution of the α and γ angles vs. pressure (Fig. 2) with the evolution of the Ca-O2 bond valence and bond length (Fig. 5) suggests that this polymerization occurs at the same pressure where the angular evolution shows a change in slope. This could imply an isosymmetric phase transition around this pressure. The relative shift of the Ca atoms is again best described in terms of cation-cation distances (Table 7). Ca occupies a cavity within the SnO_6-SiO_4 framework. In the **a**-**c** plane, the size and geometry of this cavity is defined by the positions of the SiO_4 tetrahedra, whereas in the [010] direction, it is limited by the O1 atom, which on the other hand links two consecutive SnO_6 octahedra (Fig. 7). At ambient conditions, the Ca atom is

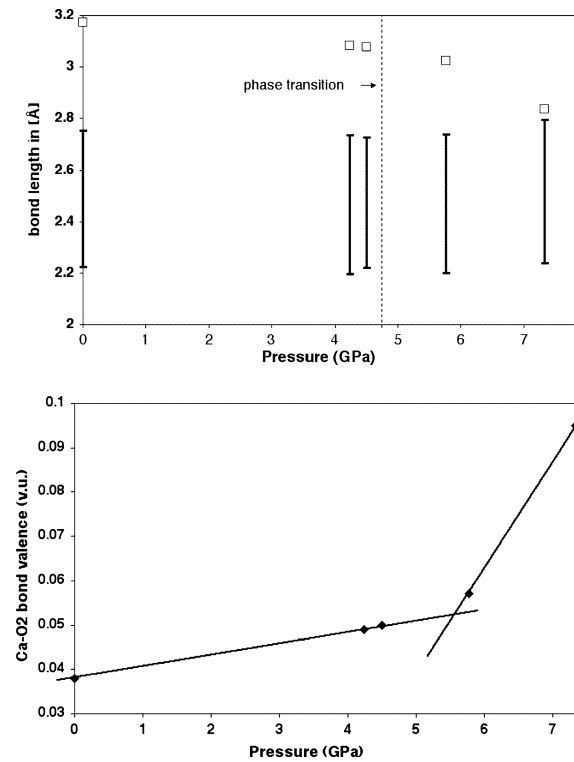

FIGURE 5. (**a**) Range of Ca-O bonds for CaO7 polyhedra (bars) compared with the approaching Ca-O2 bonds (open marks). Note that eightfold coordination is only achieved between 5.7 GPa and 7.3 GPa. (**b**) Plot of bond valences vs. pressure for Ca-O2. Note the sharp kink at ~5.8 GPa, the same pressure where a change of slope is also noticed for the cell angles versus pressure. The lines are a guide to the eye.

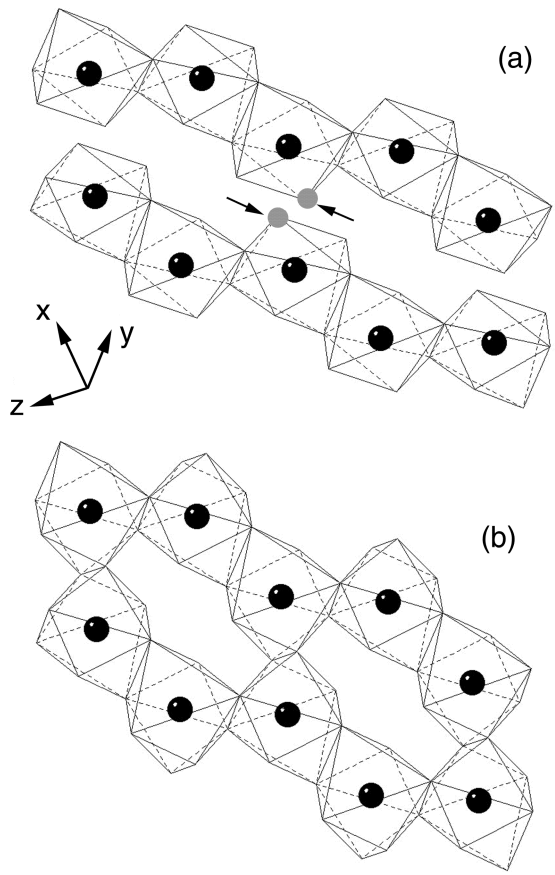

FIGURE 6. CaO7 polyhedra at room pressure (**a**) and above 5.8 GPa (**b**). The arrows indicate the oxygen atom which at high pressure connects to the neighboring chain and thus helps to form sheets parallel to $(\bar{1}11)$.

known to show an increased dynamic or static displacement within this cavity parallel to [100] as indicated by a large U_{11} value (Groat et al. 1996; Meyer et al. 1998). This thus indicates either a flat Ca potential well parallel to [100] (dynamic disorder) or two minima separated by a small energy barrier (static disorder) (Fig. 8). From the interatomic distances between Ca and Si, we can see that this flat but symmetric arrangement in the monoclinic phase is replaced by an asymmetric arrangement in the triclinic phase (Figs. 7 and 8). This is evidenced by a shortening of one Si-Ca distance approximately parallel to [100] (Table 7). It is this movement that brings one additional O2 atom, which is linked to the respective Si atom, into the coordination sphere of the Ca atom.

TABLE 7. Distances between the Ca atom and its surrounding Si atoms

Pressure (GPa)	0.000(6)	4.238(7)	4.505(4)	5.769(5)	7.33(2)
1	3.609 Å	3.570 Å	3.561 Å	3.532 Å	3.484 Å
2	3.581 Å	3.538 Å	3.530 Å	3.490 Å	3.399 Å
3	3.609 Å	3.570 Å	3.560 Å	3.562 Å	3.594 Å
4	3.581 Å	3.538 Å	3.530 Å	3.543 Å	3.609 Å

Note: The numbers 1–4 refer to the Si-labeling in Figure 7. Note the large decrease of the distance to Si-2. This causes the O2-atom coordinated to Si-2 to come into the coordination sphere of Ca and thus form a CaO_8 polyhedron.

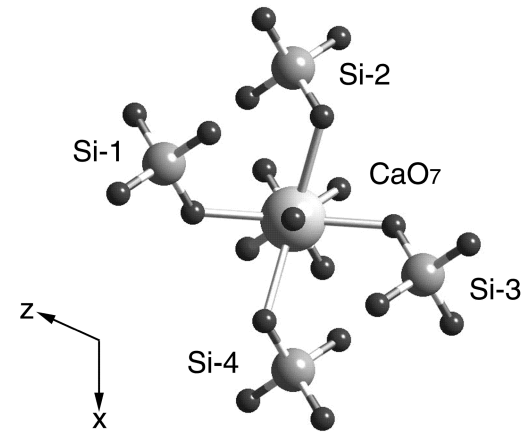

FIGURE 7. Sketch of the polyhedral environment of the Ca atom in the **a-c** plane. The Si-labels refer to the numbers in Table 7.

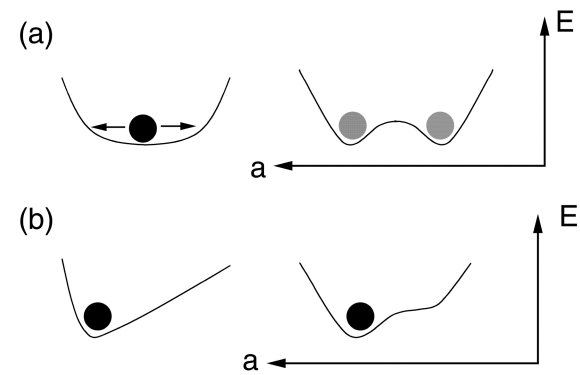

FIGURE 8. Schematic sketch of possible potential-energy curves of the Ca atom parallel [100] in the monoclinic (**a**) and triclinic (**b**) phase. Note that the large displacement parameter parallel a at ambient conditions can be explained by either a dynamic or a static disorder expressing either a flat potential well or a multiple-minima energy curve.

Comparing malayaite with titanite under non-ambient conditions

Comparing malayaite with titanite under high pressure reveals some difference in the structural evolution. First of all, titanite adopts space group *A*2/*a* at 3.6 GPa where the Ti atoms move to the geometric center of their octahedral O atom environment. Within this *A*2/*a* phase, previous experiments on titanite based on Rietveld refinements of high-pressure powder data seem to indicate a straightening of the Ti-O1-Ti angle, whereas the O1-Ti-O3 angle does not vary significantly (Kunz et al. 1996; Kunz et al. 2000). This straightening of the octahedral chains is not observed in our study on malayaite. It is not clear whether this difference is due to the different material or if it is an artifact. An artifact might result from the difficulty to accurately determine the position of O atoms especially in high-pressure data if strongly scattering atoms such as Ti are present in the structure. High-pressure studies on single crystals of titanite are currently underway.

Comparing the behavior of malayaite under pressure with other titanite-like structures

Troitzsch and Ellis (1999) reported strongly distorted SiO_4 tetrahedra at ambient conditions for the $CaTiOSiO_4$-$CaAlFSiO_4$ series. $CaAlFSiO_4$ is an Al-F analog to *A*2/*a* titanite. The Si-O2 bonds are shortened, Si-O3 bonds are elongated, and the O2-Si-O2 angle at 101.4° is very small. The authors explained this distortion with an off-centering of the Si atom, which improved the bond-valence sum of all atoms in the SiO_4 tetrahedra. The AlF_2O_4 octahedron in $CaAlFSiO_4$ remains constant upon chemical substitution. Although in malayaite the distortion of the tetrahedra is not so distinct, it seems that in this structure type, deviations from the ideal bond lengths and angles are not so exceptional in order to balance external strain imposed either by chemical exchange or non-ambient conditions.

The montebrasite-amblygonite series $Li[Al(PO_4)OH]$ – $Li[Al(PO_4)F]$ is topologically identical to the malayaite structure (Groat et al. 1990). Interestingly, these are the only known naturally occurring minerals with the titanite structure-type that crystallize in the triclinic system. Groat et al. (1990) reported them as triclinic $C\bar{1}$. A transformation matrix $\begin{pmatrix} 0 & 0 & 1 \\ 0 & 1 & 0 \\ 1 & 0 & 0 \end{pmatrix}$ reveals the identity of this structure with the high-pressure malayaite structure. The <P-O> distance in amblygonite-montebrasite remains constant across the series, but the angles deviate with increasing F/(F + OH) value. The PO_4 tetrahedra are flattened with increasing OH value similar to the SiO_4 tetrahedra in malayaite upon increasing pressure. As in triclinic malayaite, the distances between the octahedral chains are different in different directions. These differences become more pronounced with increasing OH-content. This seems to indicate that chemically imposed structural strain has a similar effect on this structure type as pressure induced strain.

The structure of $CaGe_2O_5$ can be correlated with the high-temperature structure of titanite (Aust et al. 1976) and therefore also to malayaite. Here, the Ti and Si atoms are replaced by the larger Ge atom, which reduces the symmetry at ambient conditions to $P\bar{1}$. At $T > 600$ °C $CaGe_2O_5$ adopts the monoclinic space group $C2/c$. Interestingly, Ca-O2 and Ge(6)-O2 bond lengths seem to be shortened in both the low and high symmetry phases, leading to irregular, neighboring GeO_6 octahedra.

Angel et al. (1996) described a triclinic phase for $CaSi_2O_5$. This material contains fourfold-, fivefold-, and sixfold-coordinated silicon and thus is distinctly different from the triclinic malayaite high-pressure phase. However its structure type is very similar to the aristotype of malayaite. This relationship is confirmed by a high-pressure phase transition from triclinic to monoclinic $CaSi_2O_5$, where the *A*2/*a* structure of malayaite is adopted (Angel 1997).

ACKNOWLEDGMENTS

The authors thank U. Bismayer for the kind donation of the malayaite samples. S.R. was financially supported by the ETH (project 02123). M.K. was partly supported by the Swiss National Fund (21-052682.97). Constructive comments of U.B. and R.J.A. improved this paper significantly.

REFERENCES CITED

Angel, R.J. (1997) Transformation of fivefold-coordinated silicon to the octahedral silicon in calcium silicate, CaSi2O5. American Mineralogist, 82, 836–839.

Angel, R.J., Ross, N.L., Seifert, F., and Flievoet, T.F. (1996): Structural characterisation of pentacoordinate silicon in a calcium silicate. Nature, 384, 441–444.

Angel, R.J., Allan, D.R., Miletich, R., and Finger, L.W. (1997) The use of quartz as an internal standard in high-pressure crystallography. Journal of Applied Crystallography, 30, 461–466.

Angel, R.J., Kunz, M., Miletich, R., Woodland, A.B., Koch, M., and Xirouchakis, D. (1999) High-pressure phase transition in $CaTiOSiO_4$ titanite. Phase Transitions, 68, 533–543.

Aust, H., Völlenkle, H., and Wittmann, A. (1976): Die Kristallstruktur der Hoch-und der Tieftemperaturform von CaGe2O5. Zeitschrift für Kristallographie, 144, 82–90.

Bismayer, U., Zhang, M., Groat, L.A., Salje, E.K.H., and Meyer, H.-W. (1999) The β-γ phase transition in titanite and the isosymmetric analogue in malayaite. Phase Transitions, 68, 545–556.

Burnham, C.W. (1966) Computation of absorption corrections and the significance of end effects. American Mineralogist, 51, 159–167.

Chrosch, J., Bismayer, U., and Salje, E.K.H. (1997) Anti-phase boundaries and phase transition in titanite: An X-ray diffraction study. American Mineralogist, 82, 677–681.

Grant, D.F. and Gabe, E.J. (1978) The analysis of single-crystal Bragg reflections for profile measurements. Journal of Applied Crystallography, 11, 114–120.

Groat, L.A., Raudsepp, M., Hawthorne, F.C., Ercit, T.S., Sherriff, B.L., and Hartman, J.S. (1990) The amblygonite-montebrasite series: Characterization by single-crystal structure refinement, infrared spectroscopy, and multilinear MAS-NMR spectroscopy. American Mineralogist, 75, 992–1008.

Groat, L.A., Kek, S., Bismayer, U., Schmidt, C., Krane, H.G., Meyer, H., Nistor, L., and van Tendeloo, G. (1996) A synchrotron radiation, HRTEM, X-ray powder diffraction, and Raman spectroscopic study of malayaite, $CaSnSiO_5$. American Mineralogist, 81, 595–602.

Higgins, J.B. and Ribbe, P.H. (1976) The crystal chemistry and space group of natural and synthetic titanites. American Mineralogist, 61, 878–888.

Ingham, F.T. and Bradford, E.F. (1961) First description of malayaite as an unnamed mineral. American Mineralogist, 46, 768.

Kek, S., Aroyo, M., Bismayer, U., Schmidt, C., Eichhorn, K., and Krane, H.G. (1997) The two-step phase transition of titanite, $CaTiSiO_5$: a synchrotron radiation study. Zeitschrift für Kristallographie, 212, 9–19.

King, H.E. and Finger, L.W. (1979) Diffracted beam crystal centering and its application to high-pressure crystallography. Journal of Applied Crystallography, 12, 374–378.

Kunz, M., Arlt, Ñ., and Stolz, J. (2000) In situ powder diffraction of titanite ($CaTiSiO_5$) at high pressure and high temperature. American Mineralogist, 85, 1465–1473.

Kunz, M., Xirouchakis, D., Lindsley, D.H., and Häusermann, D. (1996) High-pressure phase transition in titanite ($CaTiOSiO_4$). American Mineralogist, 81, 1527–1530.

Kunz, M., Xirouchakis, D., Wang, Y., Parise, J.B., and Lindsley, D.H. (1997) Structural investigations along the join $CaTiOSiO_4$ - $CaSnOSiO_4$. Schweizerisch Mineralogische Petrographische Mitteilung, 77, 1–11.

Malcherek, T. (2001): Spontaneous strain in synthetic titanite CaTiOSiO4. Mineralogical Magazine, 65, 709–715.

Mao, H.K., Xu, J., and Bell, P.M. (1986) Calibration of the ruby pressure gauge to 800 kbar under quasi-hydrostatic Conditions. Journal of Geophysical Research, 91, 4673–4676.

Meyer, H.-W., Bismayer, U., Adiwidjaja, G., Zhang, M., Nistor, L., and van Tendeloo, G. (1998) Natural titanite and malayaite: structural investigations and the 500K anomaly. Phase Transitions, 67, 27–49.

Miletich, R., Allan, D.R., and Kuhs, W.F. (2000) High-Pressure Single-Crystal Techniques. in: HT and HP Crystal Chemistry, Reviews in Mineralogy and Geochemistry, 41, 445–520.

Munowitz, M., Jarman, R.H., and Harrison, J.F. (1993) Theoretical study of the nonlinear optical properties of $KTiOPO_4$: Cooperative effects in the extended —Ti—O—Ti— chains. Chemistry of Materials, 5. 661–671.

Salje, E., Schmidt, C., and Bismayer, U. (1993) Structural phase transition in titanite, $CaTiSiO_5$: A ramanspectroscopic study. Physics and Chemistry of Minerals, 19, 502–506.

Sheldrick, G.M. (1997) SHELXL-97 and SHELXLS-97. Programs for crystal structure determination. University of Göttingen.

Takenouchi, S. (1971) Hydrothermal synthesis and consideration of the genesis of Malayaite. Mineralium Deposita, 6, 335–347.

Taylor, M. and Brown, G.E. (1976) High-Temperature structural study of the $P2_1/a \leftrightarrow A2/a$ phase transition in synthetic titanite, $CaTiSiO_5$. American Mineralogist, 61, 435–447.

Troitzsch, U. and Ellis, D.J. (1999) The synthesis and crystal structure of $CaAlFSiO_4$, the Al-F analog of titanite. American Mineralogist, 84, 1162–1169.

Zhang, M., Salje, E., and Bismayer, U. (1997) Structural phase transition near 825K in titanite: Evidence from infrared spectroscopic observations. American Mineralogist, 82, 30–35.

MANUSCRIPT RECEIVED APRIL 24, 2002
MANUSCRIPT ACCEPTED AUGUST 22, 2002
MANUSCRIPT HANDLED BY ALISON PAWLEY